






Communication

# How Acid Washing Nickel Foam Substrates Improves the Efficiency of the Alkaline Hydrogen Evolution Reaction

Thomas B. Ferriday<sup>1,2,\*</sup> , Suhas Nuggehalli Sampathkumar<sup>2</sup> , Peter Hugh Middleton<sup>1</sup> , Jan Van Herle<sup>2</sup>   
and Mohan Lal Kolhe<sup>1</sup> 

<sup>1</sup> Department of Engineering Science, University of Agder, NO-4879 Grimstad, Norway

<sup>2</sup> Group of Energy Materials, Swiss Federal Institute of Technology, Lausanne (EPFL), 1951 Sion, Switzerland

\* Correspondence: thomasbf@uia.no

**Abstract:** Nickel foam substrates are frequently utilised as porous 3D substrates for renewable energy applications. The preparation of these substrates usually includes an acid-washing step, but the degree to which this step affects the final electrochemical performance after spray-coating a catalyst ink is unreported. Herein, we report the effects of acid washing through physicochemical and electrochemical characterisation. The electrochemical performance was determined through repeated measurements of catalyst-coated nickel foam substrates both with and without the initial step of acid washing. It was found that acid washing increased the current density by 17.9% for the acid-treated MoS<sub>2</sub>-coated nickel foam electrode. This increment was affiliated with an electrochemically active surface area that increased by 11.2%, and a Tafel analysis indicated that the acid-treated MoS<sub>2</sub>-coated electrodes facilitated the initial water dissociation step of the hydrogen evolution reaction with greater ease. Similar effects were also discovered for acid-treated PtIr(1:3)/C-coated nickel foam substrates. The stability was also improved; the degradation rate was reduced by 18.9% for the acid-treated MoS<sub>2</sub>-coated electrodes. This demonstrates the utility of acid washing nickel foam electrodes.

**Keywords:** acid washing; nickel foam; hydrogen evolution reaction; alkaline water electrolysis; electrode preparation



**Citation:** Ferriday, T.B.; Nuggehalli Sampathkumar, S.; Middleton, P.H.; Van Herle, J.; Kolhe, M.L. How Acid Washing Nickel Foam Substrates Improves the Efficiency of the Alkaline Hydrogen Evolution Reaction. *Energies* **2023**, *16*, 2083. <https://doi.org/10.3390/en16052083>

Academic Editors: Adriano Sacco and Jin-Soo Park

Received: 3 January 2023

Revised: 19 January 2023

Accepted: 2 February 2023

Published: 21 February 2023



**Copyright:** © 2023 by the authors. Licensee MDPI, Basel, Switzerland. This article is an open access article distributed under the terms and conditions of the Creative Commons Attribution (CC BY) license (<https://creativecommons.org/licenses/by/4.0/>).

## 1. Introduction

The ongoing renewable energy transition includes new energy carriers, such as hydrogen [1–4], where production through water electrolysis yields green hydrogen. The key to this process is the hydrogen evolution reaction (HER), which is one of the two half-cell reactions in water electrolysis [5]. The advent of the novel anion exchange membrane (AEM) [1–4] has caused a shift within water electrolysis resulting in a greater emphasis on alkaline water electrolysis through AEM technology. The alkaline HER is currently under profound scrutiny, as there is considerable difficulty in finding stable catalyst materials that are capable of replacing platinum group metals (PGMs) [5]. As such, methods of improving the performance of non-PGM catalyst materials are subject to ample R&D efforts.

Chief among such methods is acid washing which is commonly featured in technologies related to water electrolysis, batteries, and general electrochemistry for electrode preparation [6–19]. The utility of acid washing is great with respect to decreasing the influence of organic contaminants and reducing the surface oxide layer. This results in a notable reduction in series resistance, thus enabling greater performances. However, there is a large disparity in the manner in which this step is carried out with respect to both acid type and concentration.

There are reports of the use of hydrochloric acid, sulphuric acid, perchloric acid, nitric acid [6–19], and likely several other options. Moreover, the concentrations vary from weak, dilute acids around 0.05 M [6,7] to undiluted acids [8–12] and everything in between [13–19]. The influence of acid washing has been characterised for use in batteries

and supercapacitors [20–22], medical implants [23], and the alkaline oxygen evolution reaction [24]. The influence of the catalyst support during hydrothermal processes for direct catalyst growth on a nickel foam support was investigated [25]. It was determined that nickel foam may indeed supply nickel ions, which may alter the catalyst composition, thus proving that the catalytic influence of the support cannot be neglected during processes such as electrodeposition. Furthermore, it follows that chemical treatments such as acid washing may affect the catalytic properties of the nickel foam support and therefore cannot be neglected.

However, the effects of acid washing nickel foam supports for the alkaline hydrogen evolution reaction remain largely unreported. Previous work displayed a notable improvement in both the series resistance and charge transfer resistance in bare nickel foam substrates that were used as alkaline HER electrodes by utilising both hydrochloric and sulphuric acid, where the latter outperformed the former [26]. Moreover, peak performance was achieved by acid washing with 0.50 M sulphuric acid, yielding a notable decline in the series resistance. However, additional physicochemical measurements detailing the changes elicited by these chemical treatments are necessary. It is highly common to apply a catalyst ink to a substrate through spray-coating, though the degree to which the aforementioned benefits of acid washing persist after spray-coating is currently unknown, and the same applies to the lifetime of such benefits. Herein, we seek to fill this void in the literature by testing multiple catalyst-coated nickel foam substrates in an efficient three-electrode setup both with and without the initial step of acid washing.

## 2. Experimental Procedure

A three-electrode setup was utilised, consisting of a nickel foam working electrode, a platinum wire counter electrode, and an extended Luggin probe (an agar salt bridge) connected to a Ag/AgCl reference electrode. The nickel foam electrode was pressed against a gold current collector to reduce the ohmic resistance, as shown in Figure 1. The small-scale setup with a fixed distance between the three electrodes allowed for a high degree of reproducibility.

The use of ionic bridges (extended Luggin probes) was essential in order to allow the reference electrodes to fit into the half-cell shown in Figure 1. These ionic bridges were produced by mixing 22.37 g of KCl (Sigma Aldrich) into 100 mL of deionised water and heating until the boiling point was reached. From here, 1.5 g (1.5 wt.%) of Difco agar (Fischer Scientific) was carefully added, thereby creating a 3.0 M KCl solution suspended in agar gel in liquid form. While the mixture was boiling, a tube attached to a syringe was employed to suck the solution into the tubing, thus filling the entire volume of both the tubing and the syringe. This was left overnight to settle, creating an ionic bridge that was ready for the insertion of Ag/AgCl (3.0 M KCl) reference electrodes the next day.

Deionised water and an appropriate quantity of potassium hydroxide (powder) for synthesis (Sigma Aldrich) were combined to create the 1.0 M KOH electrolyte, which was thoroughly hand-stirred to ensure a homogeneous concentration. The three-electrode setup was left to settle to establish a steady state by allowing the electrolyte to completely permeate all cavities of the nickel foam electrode.

The non-PGM inks were created by mixing 11 mg of MoS<sub>2</sub> powder (US Nano) with 1.5 mL of deionised water, 0.5 mL of isopropanol, and 22 mg of Sustainion<sup>®</sup> XB-7 alkaline ionomer (DiOxide Materials). This resulted in a catalyst loading of approximately 5 mg cm<sup>-2</sup><sub>MoS<sub>2</sub></sub> for the two electrodes. The PGM ink was created by distributing 3 mg of 20 wt.% PtIr(1:3)/C (fuelcellstore.com) in 1 mL of deionised water, 1.0 mL of isopropanol, and 6 mg of Sustainion<sup>®</sup> XB-7 alkaline ionomer. This resulted in a catalyst loading of approximately 0.2 mg cm<sup>-2</sup><sub>PtIr</sub> for the two electrodes. These dispersions were ultrasonicated for 15 min and spray-coated onto four 1 cm<sup>2</sup> nickel foam electrodes attached to an aluminium plate heated to approximately 80 °C. These four electrodes comprised two MoS<sub>2</sub> electrodes and two PtIr(1:3)/C electrodes; one was acid-treated and one was untreated for both types

of catalytic spray coating. Several sets of electrodes were created to allow additional control experiments to be executed.

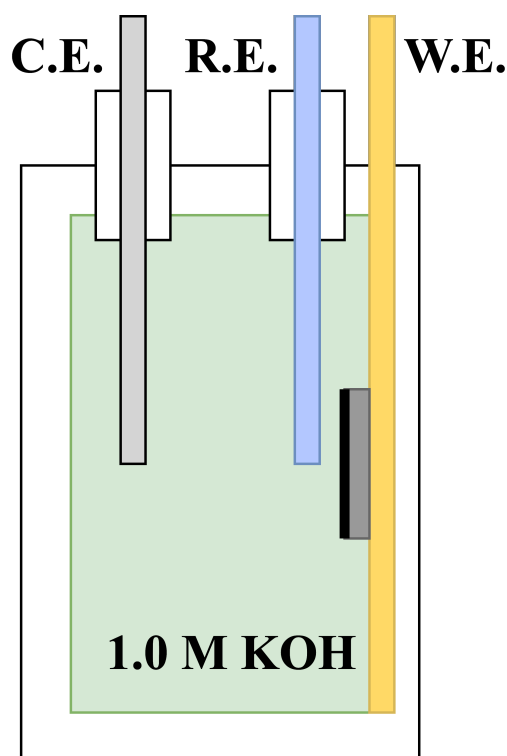


**Figure 1.** An efficient three-electrode setup with a platinum wire counter electrode (C.E.), an extended Luggin probe connected to a Ag/AgCl reference electrode (R.E.), and a catalyst-coated nickel foam working electrode (W.E.) attached to a gold plate to decrease ohmic losses. All electrochemical characterisation was performed in 1.0 M KOH at room temperature.

The electrochemical results were procured by utilising an Iviumstat electrochemical workstation. All potentials were initially measured against the Ag/AgCl reference electrode and converted to the reversible hydrogen electrode (RHE) scale using Equation (1).

$$E_{RHE} = E_{Ag/AgCl} + pH \times 0.059 + E_{Ag/AgCl}^0, \quad E_{Ag/AgCl}^0(3.0M KCl) = 0.210 V \quad (1)$$

Electrochemical impedance spectroscopy (EIS) spectra at open circuit potential were initially collected at the frequencies of  $10^5$ – $10^{-1}$  Hz with a sinusoidal perturbation of 10 mV and 10 points per decade. This was followed by polarised EIS spectra at  $-50$ ,  $-100$ ,  $-150$ , and  $-200$  mV relative to the reversible hydrogen electrode (RHE). Linear sweep voltammetry (LSV) curves were subsequently recorded between  $0.30$  and  $-0.30 V_{RHE}$  at  $10 \text{ mV s}^{-1}$  [27], and were repeated to guarantee repeatability. These data were utilised to determine the Tafel slopes. The electrochemical double layer was determined through cyclic voltammetry (CV) between  $0.346$  and  $0.446 V_{RHE}$  at scan speeds of  $10$  to  $20 \text{ mV s}^{-1}$  with  $2 \text{ mV}$  increments [28–30]. To ensure stability, the initial scan at  $10 \text{ mV s}^{-1}$  was repeated until all scans were overlapping. Stable CV results were obtained once scans at the slowest rate ( $10 \text{ mV s}^{-1}$ ) were stable. Chronopotentiometry was performed at  $10 \text{ mA cm}^{-2}$  for  $12 \text{ h}$  in  $1.0 \text{ M KOH}$  at room temperature to ascertain stability. The degradation rates were determined based on the starting point of  $-0.20 V_{RHE}$ . This sequence was repeated for all electrodes to improve the basis for comparative work, and multiple versions of each electrode type were tested to ensure stability and repeatability.

A series of physicochemical measurements were performed in order to fully understand the effect of acid washing. The surface morphology of the nickel foam electrodes was analysed in a Jeol JSM-7200F field-emission scanning electron microscope (SEM). Multiple

points were analysed with point and area-averaged analysis to ensure a solid foundation for determining the atomic composition of the surface. EDS point analysis was performed on the surface of the nickel foam, as opposed to the acid-induced pits. X-ray diffraction (XRD) was performed with a Bruker D8 Advance, and all Bragg Brentano measurements were made in reflection mode. The X-ray source was Cu  $\text{K}\alpha$  (1.5406 Å) operated at 40 kV and 40 mA (1600 W). The peaks were fitted with Fityk with a pseudo-Voigt function by using the Rietveld refinement method.

### 3. Results and Discussion

#### 3.1. Microstructural Characterisation

The effect of acid washing was ascertained through scanning electron microscopy (SEM), energy-dispersive X-ray spectroscopy (EDS), and X-ray diffraction (XRD). The effects of acid washing for increasingly potent concentrations of sulphuric acid are illustrated in Figure 2. The change in surface morphology is clear when comparing the pristine reference nickel foam in Figure 2a to the surfaces shown in Figure 2b–g. The reference nickel foam in Figure 2a presents a uniform surface with little influence of indentations, cracks or crevices. Pitting corrosion is immediately registered for the weak acid concentration of 0.01 M  $\text{H}_2\text{SO}_4$ , while any influence of uniform corrosion is not clear until the concentration is increased to 0.05 M. The degree of uniform corrosion increased together with the influence of pitting corrosion as the acid concentration was elevated, ultimately yielding surfaces where the visibility of the grain boundaries is notably reduced, as seen for 2.0 M  $\text{H}_2\text{SO}_4$  in Figure 2g. The degree of uniform surface corrosion decreased the influence of pitting corrosion due to its severity.

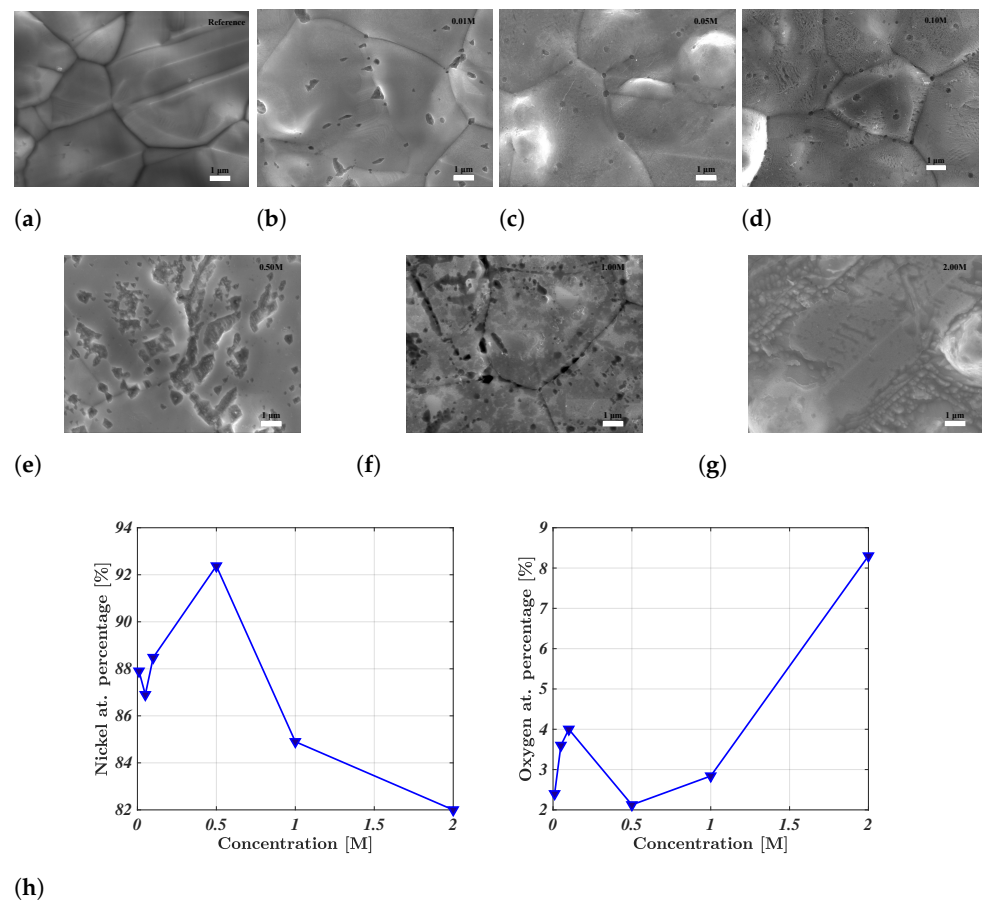


**Figure 2.** (a–g) SEM figures of the pristine  $\text{H}_2\text{SO}_4$ -treated nickel foam electrodes showing the gradual increase in surface roughness. (h) The EDS-determined atomic surface concentrations of nickel and oxygen.

The EDS results indicated a nadir/peak in the atomic percentage of oxygen/nickel, respectively, for the nickel foam electrode treated with 0.50 M sulphuric acid. This supported the results of previous work that showed a nadir for the EIS-determined series resistance for the same acid concentration [26]. Greater acid concentrations resulted in higher/lower concentrations of oxygen/nickel respectively, as shown in Figure 2h, thus agreeing with previous electrochemical evidence indicating the decreased influence of a surface oxide layer. Additional EDS point analysis of the acid-induced pits revealed a greater atomic percentage of oxygen, thus corresponding with the formation of an oxide layer, as previously noted in literature [21,22]. For large acid concentrations, the uniformity of the surface decreased simultaneously with a greater influence of oxygen. This is contradictory to the intention of acid washing, namely, to reduce the effects of surface oxides. The electrodes were exposed to air during sample mounting for SEM/EDS analysis. Thus, the increase in the surface concentration of oxygen for electrodes treated with concentrations greater than 0.50 M sulphuric acid may be related to an increased propensity to form an oxide layer once exposed to air after acid washing.

Shown in Figure 3a are the XRD spectra for select concentrations of the acid-treated nickel foam electrodes. The electrodes presented a singular cubic phase,  $fm-3m$ , where the highlighted peaks were affiliated with the 111 and 200 facets of nickel foam at  $44.61\text{--}44.69^\circ$  and  $51.96\text{--}52.07^\circ$ , respectively (JCPDS No. 87-0712) [31]. It is likely that the minor variation in peak position ( $0.08\text{--}0.11^\circ$ ) for the 0.05 M sample originated from height variations during sample mounting due to the porous nature of the nickel foam electrodes. It is clear that the width of these peaks has increased slightly with acid concentration, likely due to a decline in crystallinity owing to the formation of surface oxides during the acid washing [21,22]. A decline in crystallinity has been previously reported for HCl-treated nickel foam due to the formation of a NiO layer [21,22], where this has been noted through a gradual increment in peak width and confirmed through Raman and X-ray photoelectron spectroscopy spectra. The peaks were fitted to allow the extraction of the lattice parameters and d-spaces for the two peaks, as shown in Figure 3b. Both the lattice parameter  $a$  and the d-spacing slightly increased with increasing acid concentration. The increase in the lattice parameter  $a$  followed the same trend as that of the nickel and oxygen at.%. The change in the lattice parameter and d-spacing is likely affiliated with the aforementioned decline in crystallinity, and this would likely increase further as the acid concentration exceeded 0.50 M [21,22]. Greater lattice parameters have been affiliated with increased lattice distortion [32], where this may be due to the nickel oxide layer formed during the acid washing.

### 3.2. Electrochemical Characterisation

The following section details the results of the electrochemical characterisation. These results were procured by following the protocol detailed in the experimental section. The effects of spray-coating acid-treated nickel foam electrodes were tested for two different types of catalyst ink, namely, non-PGM  $\text{MoS}_2$  and PGM PtIr(1:3)/C. LSVs were recorded for the four types of electrodes between 0 and  $-0.30 V_{RHE}$ , as shown in Figure 4a. The peak current density for the acid-treated  $\text{MoS}_2$  and PtIr(1:3)/C electrodes increased by 17.9% and 5.19% relative to the untreated electrodes. Predictably enough, the PGM electrode surpassed the performance of the non-PGM  $\text{MoS}_2$ -coated electrode. The rationale for this performance increment was dissected by determining the electrochemical double layer  $C_{dl}$  (Figure 4b), which scales linearly with the electrochemically active surface area (ECSA). Both of the acid-treated, spray-coated electrodes displayed fair improvements relative to the regular spray-coated electrodes. However, the improvement was notably greater for the PtIr(1:3)/C-coated acid-treated electrode, where the ECSA increased by 31.8%. The ECSA of the acid-treated  $\text{MoS}_2$ -coated electrode improved by 11.2%. It is clear that the carbon black (CB)-supported catalyst experienced the greatest performance increment, which was likely due to the small particle size of the CB-supported PtIr, which enabled it to cover a greater degree of the acid-treated surface. Acid treatment with 0.50 M  $\text{H}_2\text{SO}_4$

caused notable changes to the surface, as shown in the SEM images in Figure 2, where this increased surface roughness was likely a great contributor to the augmented ECSA.

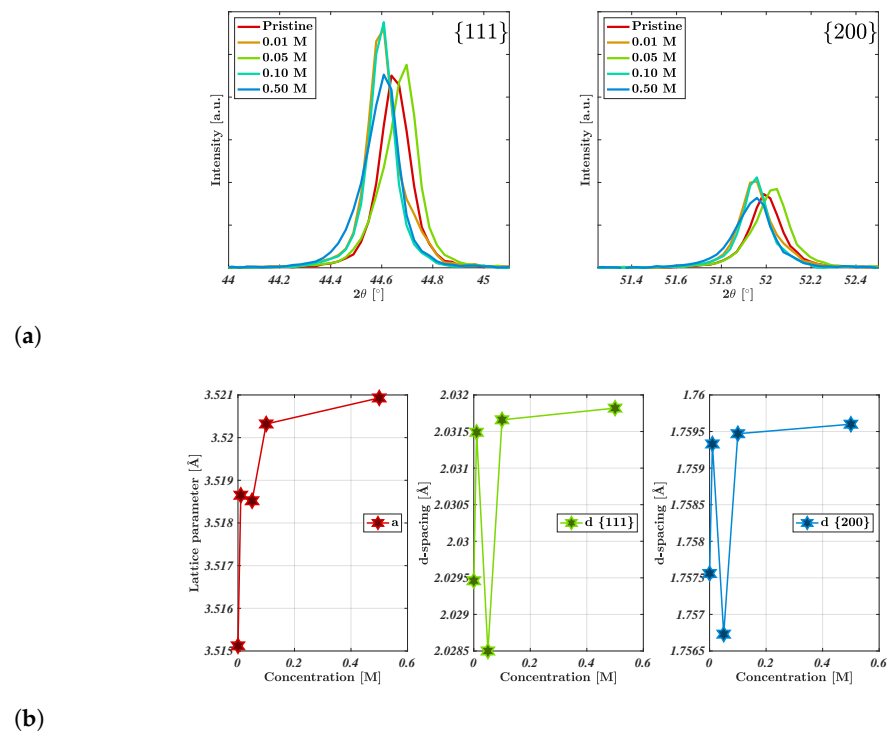


**Figure 3.** (a) XRD spectra of the acid-treated nickel foam electrodes, which are highlighted for the principal peaks related to the 111 and 200 facets, respectively. (b) The lattice parameter and d-spacing calculated from the XRD data in (a).

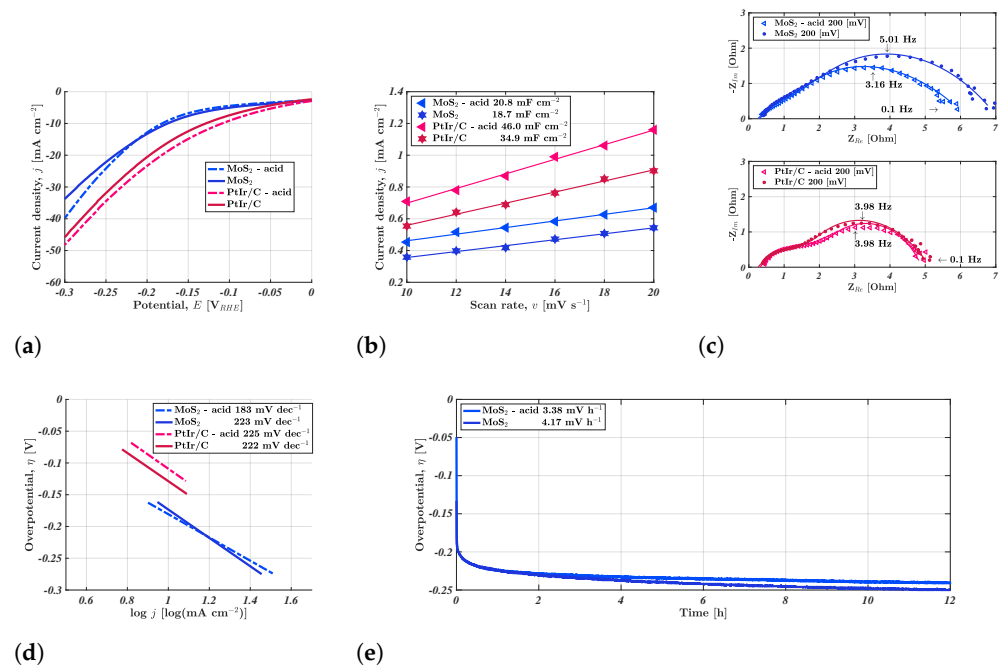


**Figure 4.** Electrochemical results detailing the effects of acid treatment on the resulting performance in 1.0 M KOH at room temperature. (a) Linear sweep voltammetry, (b) the electrochemical double layer, (c) Nyquist plots at  $-0.20$  V<sub>RHE</sub>, and (d) Tafel slopes. The stability at  $10$  mA cm<sup>-2</sup> over 12 h is shown in (e). All overpotentials are relative to the reversible hydrogen electrode.

Predictably enough, normalising the current density for the electrochemically active surface area (ECSA) revealed that the acid treatment did not notably enhance the intrinsic activity of the catalyst layer, as shown in Figure S5a. The purpose of the acid treatment was to decrease the prevalence of organic contaminants, reduce the surface oxide layer, and increase the ECSA. While there was little indication of a change in the surface oxide layer based on the series resistance shown in the polarised EIS spectra in Figure 4c, there was a clear indication of a greater ECSA, as shown by the fitted EIS curves. The EIS curves were fitted to an equivalent circuit that was typical for the HER (Figure S5c), i.e., corresponding to a faradaic reaction with one adsorbed intermediate [33]. A comparison of the double-layer capacitance from the EIS fitting revealed similar effects to those revealed by the CV scans, as shown in Table S1. The MoS<sub>2</sub>-coated acid-treated electrode displayed a fair improvement with respect to the charge transfer resistance, amounting to a 14.3% reduction. This displayed that, while the series resistance was similar, a performance increment was still achieved by reducing the charge transfer resistance. This adhered to established trends in prior research [26] where acid treatment reduced the series resistance, though the decline in charge transfer resistance was greater. Both versions of the PtIr(1:3)/C-coated electrodes displayed similar total impedance spectra, though there was a slight change in capacitance, which correlated with the 31.8% improvement in  $C_{dl}$ .

The Tafel curves in Figure 4d show that the MoS<sub>2</sub>-coated acid-treated electrode underwent a reduction in the Tafel slope, while the affiliated slopes of both versions of the PtIr(1:3)/C were largely similar to each other. Moreover, the MoS<sub>2</sub>-coated untreated electrode displayed a Tafel slope that was very similar to those of the PtIr(1:3)/C-coated electrodes. The Volmer reaction (water dissociation) is the rate-determining step for Tafel slopes equal to or greater than 120 mV dec<sup>-1</sup> for the HER [5]. As such, the reduction in the Tafel slope for the MoS<sub>2</sub>-coated acid-treated electrode indicated an improved pathway for hydrogen evolution, and the use of the acid treatment would appear to improve the efficiency of this step.

The stability of these improvements was tested by performing CP, as shown in Figure 4e, and the degradation rate of the MoS<sub>2</sub>-coated acid-treated electrode was lower than that of the untreated version of the non-PGM HER electrode. The 18.9% lower degradation rate (3.38 mV h<sup>-1</sup>) showed that the improvements induced by the acid treatment did not immediately abate during continuous operation. This indicates the possibility of greater longevity when including the initial acid-washing step prior to catalyst coating.

#### 4. Conclusions

This paper investigated how acid washing nickel foam substrates affects the performance and stability of the electrodes after they have been spray-coated with a catalytic ink. The electrochemical performance of catalyst-coated nickel foam was evaluated for both acid-treated and untreated nickel foam for two types of catalytic ink. By employing MoS<sub>2</sub>- or PtIr(1:3)/C-coated nickel foam as a hydrogen evolution reaction electrode in 1.0 M KOH, it was clear that the acid washing positively affected the performance of both types of HER electrodes. The LSV performance of the acid-treated MoS<sub>2</sub>- and PtIr(1:3)/C-coated electrodes increased by 17.9% and 5.19%, respectively. This was correlated with an augmented ECSA, as shown by the CV and EIS spectra. A great ECSA improvement was noted for the MoS<sub>2</sub>-coated electrode, which increased by 11.2%. The Tafel analysis indicated an improvement in the water dissociation step, which likely contributed to the enhanced LSV performance. The stability also appeared to increase after acid washing, as the degradation rate was lowered by 18.9%. These results demonstrate the utility of acid washing substrates prior to the application of a catalyst layer.

**Supplementary Materials:** The following supporting information can be downloaded at: <https://www.mdpi.com/article/10.3390/en16052083/s1>, Figure S1: Additional SEM figures for the various acid treated nickel foam electrodes.; Figure S2: Additional SEM figures for the various acid treated nickel foam electrodes.; Figure S3: Complete EDS scan with quantification for the various acid treated nickel foam electrodes.; Figure S4: Cyclic voltammetry scans performed in a non-faradaic

region. These were utilised to determine the double layer capacitance for catalyst-coated, acid treated nickel foam electrodes.; Figure S5: The performance of the untreated and acid treated electrodes quantified through (a) linear sweep voltammograms measured in pseudo-steady state ( $10 \text{ mV s}^{-1}$ ) [27] normalised for the ECSA determined by cyclic voltammetry. (b) Fitted open circuit EIS spectra. (c) The equivalent circuit employed to fit the EIS spectra.; Table S1: Values from the fitting of EIS spectra to the equivalent circuit displayed in Figure S5c. References [27,29,30,34] are cited in the supplementary materials.

**Author Contributions:** Conceptualisation, T.B.F. and S.N.S.; methodology, T.B.F. and S.N.S.; software, T.B.F.; validation, T.B.F. and S.N.S.; formal analysis, T.B.F. and S.N.S.; investigation, T.B.F.; resources, P.H.M., J.V.H. and M.L.K.; data curation, T.B.F.; writing—original draft preparation, T.B.F.; writing—review and editing, T.B.F. and S.N.S.; visualisation, T.B.F.; supervision, P.H.M., J.V.H. and M.L.K.; project administration, P.H.M., J.V.H. and M.L.K.; funding acquisition, P.H.M., J.V.H. and M.L.K. All authors have read and agreed to the published version of the manuscript.

**Funding:** This research received no external funding.

**Data Availability Statement:** Data may be made available upon request.

**Conflicts of Interest:** The authors declare no conflict of interest.

## References

1. Ferriday, T.; Middleton, P. Alkaline fuel cell technology—A review. *Int. J. Hydrog. Energy* **2021**, *46*, 18489–18510. [[CrossRef](#)]
2. Ferriday, T.; Middleton, P. 4.07—Alkaline Fuel Cells, Theory and Applications. In *Comprehensive Renewable Energy*, 2nd ed.; Letcher, T., Ed.; Elsevier: Oxford, UK, 2022; pp. 166–231.
3. Vincent, I.; Lee, E.C.; Kim, H.M. Comprehensive impedance investigation of low-cost anion exchange membrane electrolysis for large-scale hydrogen production. *Sci. Rep.* **2021**, *11*, 293. [[CrossRef](#)] [[PubMed](#)]
4. Varcoe, J.; Atanassov, P.; Dekel, D.; Herring, A.; Hickner, M.; Kohl, P.; Kucernak, A.; Mustain, W.; Nijmeijer, K.; Scott, K.; et al. Anion-exchange membranes in electrochemical energy systems. *Energy Environ. Sci.* **2014**, *7*, 3135–3191. [[CrossRef](#)]
5. Ferriday, T.; Middleton, P.; Kolhe, M. Review of the Hydrogen Evolution Reaction—A Basic Approach. *Energies* **2021**, *14*, 8535. [[CrossRef](#)]
6. Akhtar, N.; El-Safty, S.; Khairy, M.; El-Said, W. Fabrication of a highly selective nonenzymatic amperometric sensor for hydrogen peroxide based on nickel foam/cytochrome c modified electrode. *Sens. Actuators B Chem.* **2015**, *207*, 158–166. [[CrossRef](#)]
7. Dong, S.; Ji, X.; Yu, M.; Xie, Y.; Zhang, D.; He, X. Direct synthesis of interconnected porous carbon nanosheet/nickel foam composite for high-performance supercapacitors by microwave-assisted heating. *J. Porous Mater.* **2018**, *25*, 923–933. [[CrossRef](#)]
8. Chaudhari, N.; Jin, H.; Kim, B.; Lee, K. Nanostructured materials on 3D nickel foam as electrocatalysts for water splitting. *Nanoscale* **2017**, *9*, 12231–12247. [[CrossRef](#)]
9. Zhang, C.; Du, X.; Wang, Y.; Han, X.; Zhang, X. NiSe<sub>2</sub>@Ni<sub>x</sub>S<sub>y</sub> nanorod on nickel foam as efficient bifunctional electrocatalyst for overall water splitting. *Int. J. Hydrog. Energy* **2021**, *46*, 34713–34726. [[CrossRef](#)]
10. Lu, L.; Hou, D.; Fang, Y.; Huang, Y.; Ren, Z. Nickel based catalysts for highly efficient H<sub>2</sub> evolution from wastewater in microbial electrolysis cells. *Electrochim. Acta* **2016**, *206*, 381–387. [[CrossRef](#)]
11. Ji, B.; Zhao, W.; Duan, J.; Fu, L.; Ma, L.; Yang, Z. Immobilized Ag<sub>3</sub>PO<sub>4</sub>/GO on 3D nickel foam and its photocatalytic degradation of norfloxacin antibiotic under visible light. *RSC Adv.* **2020**, *10*, 4427–4435. [[CrossRef](#)]
12. Pierozynski, B.; Mikolajczyk, T.; Kowalski, I. Hydrogen evolution at catalytically-modified nickel foam in alkaline solution. *J. Power Sources* **2014**, *271*, 231–238. [[CrossRef](#)]
13. He, Z.; Sun, J.; Wei, J.; Wang, Q.; Huang, C.; Chen, J.; Song, S. Effect of silver or copper middle layer on the performance of palladium modified nickel foam electrodes in the 2-chlorobiphenyl dechlorination. *J. Hazard. Mater.* **2013**, *250–251*, 181–189. [[CrossRef](#)] [[PubMed](#)]
14. Shih, Y.J.; Wu, Z.L.; Huang, Y.H.; Huang, C.P. Electrochemical nitrate reduction as affected by the crystal morphology and facet of copper nanoparticles supported on nickel foam electrodes (Cu/Ni). *Chem. Eng. J.* **2020**, *383*, 123157. [[CrossRef](#)]
15. Sarawutanukul, S.; Phattharasupakun, N.; Wutthiprom, J.; Sawangphruk, M. 3D CVD graphene oxide on Ni foam towards hydrogen evolution reaction in acid electrolytes at different concentrations. *ECS Trans.* **2018**, *85*, 49.
16. Lu, X.; Pan, J.; Lovell, E.; Tan, T.; Ng, Y.; Amal, R. A sea-change: Manganese doped nickel/nickel oxide electrocatalysts for hydrogen generation from seawater. *Energy Environ. Sci.* **2018**, *11*, 1898–1910. [[CrossRef](#)]
17. Li, X.; Zhang, Z.; Xiang, Q.; Chen, R.; Wu, D.; Li, G.; Wang, L. A three-dimensional flower-like NiCo-layered double hydroxide grown on nickel foam with an MXene coating for enhanced oxygen evolution reaction electrocatalysis. *RSC Adv.* **2021**, *11*, 12392–12397. [[CrossRef](#)]
18. Bai, J.; Sun, Q.; Wang, Z.; Zhao, C. Electrodeposition of cobalt nickel hydroxide composite as a high-efficiency catalyst for hydrogen evolution reactions. *J. Electrochem. Soc.* **2017**, *164*, H587. [[CrossRef](#)]
19. Dastafkan, K.; Li, Y.; Zeng, Y.; Han, L.; Zhao, C. Enhanced surface wettability and innate activity of an iron borate catalyst for efficient oxygen evolution and gas bubble detachment. *J. Mater. Chem. A* **2019**, *7*, 15252–15261. [[CrossRef](#)]



20. Ansari, S.; Parveen, N.; Al-Othoum, M.; Ansari, M. Effect of washing on the electrochemical performance of a three-dimensional current collector for energy storage applications. *Nanomaterials* **2021**, *11*, 1596.
21. Yu, M.; Wang, W.; Li, C.; Zhai, T.; Lu, X.; Tong, Y. Scalable self-growth of Ni@NiO core-shell electrode with ultrahigh capacitance and super-long cyclic stability for supercapacitors. *NPG Asia Mater.* **2014**, *6*, e129.
22. Bakar, N.A.A.; Salleh, N.A.; Hamid, N.A.A.; Abdullah, C.A.C.; Rahiman, W.; Basirun, W.J.; Kheawhom, S.; Mohamad, A.A. The effect different of hydrochloric acid concentrations on the cleaning of Ni foam substrate: Structural and morphological studies. *Mater. Today: Proc.* **2022**, *60*, 1036–1041. [[CrossRef](#)]
23. Hung, K.Y.; Lin, Y.C.; Feng, H.P. The Effects of Acid Etching on the Nanomorphological Surface Characteristics and Activation Energy of Titanium Medical Materials. *Materials* **2017**, *10*, 1164. [[CrossRef](#)] [[PubMed](#)]
24. Kim, M.; Kim, J.; Qin, L.; Mathew, S.; Han, Y.; Li, O.L. Gas-Liquid Interfacial Plasma engineering under dilute nitric acid to improve hydrophilicity and OER performance of nickel foam. *Prog. Nat. Sci. Mater. Int.* **2022**, *32*, 608–616. [[CrossRef](#)]
25. Bu, X.; Wei, R.; Cai, Z.; Quan, Q.; Zhang, H.; Wang, W.; Li, F.; Yip, S.; Meng, Y.; Chan, K.; et al. More than physical support: The effect of nickel foam corrosion on electrocatalytic performance. *Appl. Surf. Sci.* **2021**, *538*, 147977. [[CrossRef](#)]
26. Ferriday, T.B.; Sampathkumar, S.N.; Middleton, P.H.; Van Herle, J. Investigation of Wet-Preparation Methods Of Nickel Foam For Alkaline Water Electrolysis. *J. Phys. Conf. Ser.* **2023**, *2430*, 012002. [[CrossRef](#)]
27. Pletcher, D.; Greff, R.; Peat, R.; Peter, L.M.; Robinson, J. Steady state and potential step techniques. In *Instrumental Methods in Electrochemistry*; Elsevier: Amsterdam, The Netherlands, 2001; pp. 42–76.
28. Roy, S.B.; Akbar, K.; Jeon, J.H.; Jerng, S.-K.; Truong, L.; Kim, K.; Yi, Y.; Chun, S.-H. Iridium on vertical graphene as an all-round catalyst for robust water splitting reactions. *J. Mater. Chem. A* **2019**, *7*, 20590–20596. [[CrossRef](#)]
29. Kim, H.; Oh, S.; Cho, E.; Kwon, H. 3D porous cobalt–iron–phosphorus bifunctional electrocatalyst for the oxygen and hydrogen evolution reactions. *ACS Sustain. Chem. Eng.* **2018**, *6*, 6305–6311.
30. Connor, P.; Schuch, J.; Kaiser, B.; Jaegermann, W. The Determination of Electrochemical Active Surface Area and Specific Capacity Revisited for the System MnO<sub>x</sub> as an Oxygen Evolution Catalyst. *Z. Phys. Chem.* **2020**, *234*, 979–994. [[CrossRef](#)]
31. Long, L.; Yao, Y.; Yan, M.; Wang, H.; Zhang, G.; Kong, M.; Yang, L.; Liao, X.; Yin, G.; Huang, Z. Ni<sub>3</sub>S<sub>2</sub>@polypyrrole composite supported on nickel foam with improved rate capability and cycling durability for asymmetric supercapacitor device applications. *J. Mater. Sci.* **2017**, *52*, 3642–3656. [[CrossRef](#)]
32. Niu, J.; Liu, X.; Xia, K.; Xu, L.; Xu, Y.; Fang, X.; Lu, W. Effect of electrodeposition parameters on the morphology of three-dimensional porous copper foams. *Int. J. Electrochem. Sci* **2015**, *10*, 7331–7340.
33. Lasia, A. Electrochemical impedance spectroscopy and its applications. In *Modern Aspects of Electrochemistry*; Springer: Berlin/Heidelberg, Germany, 2002; pp. 131–137.
34. Wang, N.; Xu, A.; Ou, P.; Hung, S.-F.; Ozden, A.; Lu, Y.-R.; Abed, J.; Wang, Z.; Yan, Y.; Sun, M.-J.; et al. Boride-derived oxygen-evolution catalysts. *Nat. Commun.* **2021**, *12*, 6089. [[CrossRef](#)] [[PubMed](#)]

**Disclaimer/Publisher’s Note:** The statements, opinions and data contained in all publications are solely those of the individual author(s) and contributor(s) and not of MDPI and/or the editor(s). MDPI and/or the editor(s) disclaim responsibility for any injury to people or property resulting from any ideas, methods, instructions or products referred to in the content.